Palaeoproterozoic oxygenated oceans following the Lomagundi–Jatuli Event

Kaarel Mänd, Stefan Lalonde, Leslie Robbins, Marie Thoby, Kärt Paiste, Timmu Kreitsmann, Päärn Paiste, Christopher Reinhard, Alexandr Romashkin, Noah J. Planavsky, et al.

Paleoproterozoic oxygenated oceans following the Lomagundi-Jatuli Event

Kaarel Mänd[a, b]*, Stefan V. Lalonde[c], Leslie J. Robbins[d], Marie Thoby[c], Kärt Paiste[e], Timmu Kreitsmann[b], Päärn Paiste[b], Christopher T. Reinhard[f, g], Alexander E. Romashkin[h], Noah J. Planavsky[d], Kalle Kirsimäe[b], Aivo Lepland[b, e, i], Kurt O. Konhauser[a]

[a]Department of Earth & Atmospheric Sciences, University of Alberta, Edmonton, AB T6G 2E3, Canada.

[b]Department of Geology, University of Tartu, Ravila 14A, 50411 Tartu, Estonia.

[c]CNRS–UMR6538 Laboratoire Géosciences Océan, European Institute for Marine Studies, UBO, 29280 Plouzané, France.

[d]Department of Geology & Geophysics, Yale University, New Haven, CT 06511, USA.

[e]CAGE—Centre for Arctic Gas Hydrate, Environment and Climate, Department of Geosciences, UiT The Arctic University of Norway, 9037 Tromsø, Norway.

[f]School of Earth and Atmospheric Sciences, Georgia Tech, Atlanta, GA 30332, USA.

[g]NASA Astrobiology Institute Alternative Earths Team, University of California, Riverside, CA 9252, USA.

[h]Institute of Geology, Karelian Science Centre, Pushkinskaya 11, 185610 Petrozavodsk, Russia.

[i]Geological Survey of Norway (NGU), 7491 Trondheim, Norway.

*Corresponding author: E-mail kaarel.mand@ualberta.ca.

The ~2220–2060 Ma Lomagundi-Jatuli Event (LJE) was the longest positive carbon isotope excursion in Earth history and is traditionally interpreted to reflect increased organic carbon burial and a transient rise in atmospheric O_2. However, it is widely held that O_2 levels collapsed for more than a billion years following the LJE. Here, we show that black shales postdating the LJE from the ~2000 Ma Zaonega Formation (ZF) contain the highest redox-sensitive trace metal concentrations reported in sediments deposited before the Neoproterozoic. This unit also contains the most positive shale U isotope ($\delta^{238}U$) values measured to date, providing novel evidence that there was a transition to modern-like biogeochemical cycling during the Paleoproterozoic. Although these records do not preclude a return to anoxia during the Paleoproterozoic, they uniquely suggest that the oceans remained well-oxygenated millions of years after the termination of the LJE.

The Paleoproterozoic era (2500–1600 Ma) witnessed the longest positive carbon ($\delta^{13}C_{carb}$) isotope excursion in Earth's history, recorded in marine carbonates deposited worldwide between ~2220–2060 Ma—the Lomagundi-Jatuli Event (LJE)[1,2]. Marine carbonates are generally characterized by $\delta^{13}C_{carb}$ values that vary between −5‰ to 5‰ for most of Earth's history, whereas peak LJE $\delta^{13}C_{carb}$ values reach 10–15‰[1,3,4]. There is ongoing debate regarding the processes that led to the LJE. The standard and most commonly accepted interpretation invokes increased burial of ^{13}C-depleted organic carbon (C_{org}), leading to the ^{13}C-enrichment of the dissolved inorganic carbon pool and positive $\delta^{13}C_{carb}$[3,4]. This acceleration in C_{org} burial may have been the result of an increase in oxidative weathering and nutrient delivery to the oceans[4]. Using a simple isotope mass balance, it has been estimated that between $5–9\times10^{20}$ mol of C_{org} was buried over 100 Ma, corresponding to the release of O_2 equivalents representing 12–22 times the present O_2 atmospheric pool. An ensemble of evidence points to atmospheric O_2 accumulation during the LJE, including proxies indicating growth of the marine sulphate reservoir[7–9], elevated concentrations of redox sensitive elements (RSE)[10–13], and evidence for locally oxic conditions[4,15]. However, others have argued that the 'standard' interpretation of the LJE is difficult to reconcile with our understanding of the C and O cycles[16–18], and that there is a notable paucity of C_{org}-rich deposits at this time[19], the most basic tracer of enhanced organic carbon burial. Further, the carbon isotope dynamics during and after the positive excursion are currently debated, and there

are multiple interpretations of the LJE positive $\delta^{13}C_{carb}$ values that do not invoke elevated rates of organic carbon burial and oxygen release (ref 18). Therefore, additional constraints on carbon and oxygen cycling are clearly needed to refine our view of this time interval.

In this work we present new redox tracer data from three correlative cores (OnZaP-1, 3 and OPH) of the upper Zaonega Formation (ZF), a mudstone-dolostone succession deposited in the aftermath of the LJE. We provide some of the most straightforward evidence for Proterozoic surface oxygenation. In fact, current redox proxy records are most consistent with increasing oxygenation in the aftermath of the LJ positive carbon isotope excursion—forcing a re-evaluation of our basic view of this turbulent interval of Earth's history.

Age and geochemical signatures of the Zaonega Formation

According to the latest U-Pb age constraints on tuff horizons within the lower ZF, the formation was deposited at <1970 Ma, ~70 Myrs after the proposed termination of the LJE[28]. This age model is consistent with $\delta^{13}C_{carb}$ stratigraphy. In the Onega Basin, $\delta^{13}C_{carb}$ values in the lowermost ZF and underlying Tulomozero Formation are characterized by typical LJE values of ≥8‰[29], with $\delta^{13}C_{carb}$ in preserved carbonate strata returning to normal marine values of ~0‰ further upsection[30]. In the OPH core, the studied section occurs after several hundred meters of stratigraphy—including cumulatively ~210 meters of mudstone-dominated sediments—and contains carbonates bearing a negative or normal marine (and therefore post-LJE) $\delta^{13}C_{carb}$ signal (ref. 30). Assuming a reasonable range of deposition rates for the mudstones—e.g., 1–100 m Myr^{-1} (Sadler et al., 1999, GeoResearch Forum.)—the studied section of the ZF was deposited millions of years after the termination of the LJE in the Onega Basin.

The section is rich in total organic carbon (TOC), with average values of 27.4±18.5 wt.% in mudstones of the OnZaP-1 and 3 cores (combined into the OnZaP section, see Methods), and 14.5±9.9 wt.% in OPH mudstones (Figure 1). These values are roughly comparable to the most organic-rich modern marine sediments (e.g., up to 21.3 wt.% on the Peru margin; Böning et al., 2004, GCA). Molybdenum, uranium (U), and rhenium (Re) concentrations in Zaonega mudstones are significantly elevated relative to other Proterozoic black shales[11,13,26], averaging 130±142 μg g^{-1}, 19±15 μg g^{-1}, and 116±84 ng g^{-1}, respectively, in OnZaP mudstones. In the OPH section, Mo

and U average 71±92 μg g^{-1} and 37±50 μg g^{-1}, whereas overall maximum Mo, U, and Re concentrations across both sites are 1009 μg g^{-1}, 238 μg g^{-1}, and 516 ng g^{-1}, respectively. We focus specifically on Mo, U, and Re enrichments, as these metals have previously provided robust evidence for major shifts in Earth's redox state[11,13,26]. In the OnZaP section, $\delta^{98/95}$Mo is on average 0.67±0.81‰, with a maximum of 1.49±0.14‰. Uranium isotope values in the OnZaP section range from −0.03 to 0.79‰, with an average of 0.47‰. The maximum value is the most ^{238}U-enriched shale value that has been reported to date (ref. 76, Yang et al., 2017, Precambrian Res.).

The primary source of these RSE to the oceans is the oxidative weathering of terrestrial RSE-bearing minerals (e.g., pyrite, uraninite), and subsequent riverine transport as aqueous oxyanions[34,35]. Hydrothermal inputs, while not fully constrained at present, are not expected to be a quantitatively significant source for any of these RSE[26,35]. The most important sink for these RSE is sequestration into marine sediments, which is influenced by the redox state of the depositional setting[34,36]. In oxic seawater, these RSE are present as recalcitrant species that tend to accumulate in the water column[35,37], although Mo adsorbs to Mn(IV)-oxides under oxic conditions and can then be released in pore waters following the reductive dissolution of Mn(IV)-oxides in anoxic sediments[38]. In anoxic environments, these RSE are progressively converted into particle-reactive species resulting in efficient drawdown through authigenic sulphide precipitation or adsorption to organic matter[36,37]. With regards to Mo, it has been found that most efficient Mo sequestration takes place under euxinic waters with >11 μM of sulphide (HS^-)[39]. In a broad sense, the contrasting behaviour of these elements in oxic and anoxic conditions ensures that the drawdown and marine reservoir sizes are governed by global ocean redox—large reservoirs of these RSE develop in an oxic ocean, which leads to large local sedimentary RSE enrichments under anoxic conditions[13,26].

The U and Mo isotope systems, similar to RSE enrichments, respond to the global marine redox landscape. There is consensus that well-oxygenated oceans are characterized by heavy Mo and U isotope values (ref. 71 and Andersen et al., 2017, Rev. Mineral. Geochem.). It is, however, difficult to gauge when a sedimentary archive captures seawater U and Mo isotope values. For instance, it is easiest to capture seawater Mo isotope values in shales deposited in isolated basins with high HS^- levels (ref. 50), but euxinic marine basins often deviate from the seawater isotope composition (ref. 71)—$\delta^{98/95}$Mo in euxinic shales is therefore often interpreted as a minimum

111 estimate for seawater (ref. 15). Uranium isotope values in shales will be closest to seawater
112 values in oxic sediments and up to ~1‰ heavier than seawater in anoxic and high productivity
113 settings (Andersen et al., 2014, EPSL) (see SI for detailed discussion on Mo and U isotope values).
114 Using this framework, our data points to well-oxygenated oceans with high rates of primary
115 productivity during deposition of the Zaonega Formation.

116 ## Marine RSE inventory

117 Enrichments in RSE (in the rest of this manuscript, RSE refers specifically to Mo, U, and Re) in the
118 ZF far exceed anything known from pre-Neoproterozoic black shales (Figure 2). Similar values
119 are found only in the Phanerozoic, where they have been taken as evidence for an expanded
120 seawater RSE inventory, the direct result of pervasive ocean-atmosphere oxygenation[11,13,26]. We
121 believe that the ZF, likewise, contains evidence of a large marine RSE inventory that strongly
122 suggests a relatively oxidized ocean–atmosphere system with a robust terrestrial oxic RSE
123 weathering flux, in which the drawdown of RSE was limited by the relative scarcity of anoxic
124 conditions on the seafloor. Further, U and Re enrichments—which, unlike Mo, are also drawn
125 down in ferruginous waters[48]—suggest that this was an episode of thorough water column
126 oxygenation on continental shelves, rather than just a restriction of euxinic deposition, >1.4 Gyr
127 before terminal oceanic oxygenation during the Neoproterozoic[42].

128 While low Mo in black shales could be explained by either a small marine Mo pool, basinal
129 restriction leading to localized Mo depletion[38], or inefficient Mo scavenging under low HS^-
130 conditions[39], there are limited ways to explain elevated RSE concentrations in black shales of the
131 ZF (i.e., up to several hundreds of μg g^{-1} of Mo throughout the >160 km-wide basin). One
132 possibility is anomalously low sedimentation rates, which have previously been invoked to
133 explain high TOC in U-rich black shales of the Miocene Monterey Formation, USA[47]. Although low
134 sedimentation rates may have played a role in concentrating TOC and RSE in the ZF, the
135 magnitude of the RSE enrichment—consistent with Phanerozoic levels (Figure 2)—makes it
136 unlikely sedimentation rate alone could account for it. A more plausible explanation is that the ZF
137 was also a highly efficient RSE sink that had reliable access to a large oceanic RSE inventory[38,43]
138 (see SI for additional discussion on factors controlling RSE accumulation).

The U isotope values provide an independent confirmation of highly oxygenated oceans—as noted above they are the most positive shale $\delta^{238}U$ values reported to date (Figure 2), requiring both heavy seawater $\delta^{238}U$ values (likely comparable to the modern value of ~–0.4‰) and a relatively full expression of the equilibrium ~1.2‰ fractionation during U reduction**.** Heavy seawater values only develop when oxic U burial is a major U burial flux in well-oxygenated oceans (Andersen, 2014). In addition, a significant positive U isotope fractionation (>0.6‰) strongly suggests U reduction in the water column (Andersen, 2017, Rev. Mineral. Geochem.). Uranium reduction rates appear to scale with sulphate (or iron) reduction rates (Barnes and Cochran, 1993, GCA)—providing a link between amounts of organic matter loading in a marine system and the isotope fractionation that occurs during U burial. For reference, there is limited water column sulphate reduction in the modern Black Sea and Cariaco Basin because of low rates of productivity and maximum sediment $\delta^{238}U$ values are ~0.4‰ and 0.2‰, respectively (Andersen, 2014, EPSL). Therefore, these strongly positive U isotope values, along with the RSE enrichments, are most readily explained by invoking both globally well-oxygenated oceans and markedly elevated rates of local primary productivity, the latter of which would tend to enhance the expression of isotope effects associated with U reduction.

Conflicting views on oxygenation during ZF deposition

Our interpretation that the ZF records well-oxygenated ocean conditions is ostensibly in conflict with previous interpretations derived from C, S, and Mo isotope records proposed to reflect global deoxygenation. However, much of this data can plausibly be explained through local rather than global processes. First, Kump *et al.*[19] postulated a post-LJE global negative $\delta^{13}C$ excursion based on depleted $\delta^{13}C$ in ZF carbonates. This was interpreted to result from the widespread oxidation of organic-rich shales, which would have favoured suppressed, rather than elevated, O_2 levels. However, negative $\delta^{13}C$ in the ZF has subsequently been reinterpreted to reflect basin-wide methanotrophy and secondary overprinting of carbonate rocks[49]. Second, Scott *et al.*[8] argued that highly ^{34}S-enriched pyrites in the upper ZF reflect a global collapse of the marine sulphate reservoir due to deoxygenation. In contrast, Paiste *et al.*[27] explained the same trends through basin-specific processes involving quantitative uptake of sulphate. Third, Asael *et al.*[14] inferred an ~0.7‰ seawater $\delta^{98/95}Mo$ value from two other cores in the upper ZF, identical to

the average in the OnZaP section. Mn-oxides, which form in oxic waters, preferentially scavenge ^{95}Mo and drive seawater $\delta^{98/95}$Mo to higher values. If one assumes a modern riverine input value of ~0.7‰ for the Paleoproterozoic (ref. 71), a seawater value of ~0.7‰ suggests limited Mn-oxide precipitation and, thus, little O_2 in the oceans. However, as outlined above, the sequestration of Mo in sediments commonly imparts a negative $\delta^{98/95}$Mo fractionation (ref. 71). This highlights that the highest Mo isotope values of ~1.4‰ represent a minimum seawater $\delta^{98/95}$Mo estimate (see ref. 15 and SI) and that the Mo isotope data does not necessarily preclude widespread oxic conditions.

Implications of oxygenated oceans at ~2.0 Ga

RSE-replete conditions during the deposition of the ZF have important implications for Earth's global C and O cycles during the Paleoproterozoic. Tracking the evolution of Earth's redox history is also critical for understanding early eukaryote evolution. The late rise to prevalence of eukaryotes in the Neoproterozoic is thought to be linked to widespread anoxic and nutrient-poor conditions that favoured prokaryotic metabolisms[55,56]. Given the extent of ocean oxygenation and nutrient abundance inferred from the ZF[4,44], conditions favourable to eukaryotic diversification could have been present for much of the middle Paleoproterozoic. It is curious, then, that molecular clock analyses and microfossil evidence of eukaryote origin tend to converge after ~1900 Ma[57,58]. In the simplest sense this discrepancy supports the central importance of a unique endosymbiosis event for the emergence of eukaryotes, rather than removal or lessening of an environmental barrier.

The ZF is part of a well-recognized overall trend towards elevated RSE concentrations at ~2400–2000 Ma that has been linked to well-oxygenated oceanic–atmospheric conditions[11–13]. However, surprisingly our ZF data extend this trend past the termination of the LJE. Furthermore, the extreme RSE enrichments hint that, instead of being in decline, atmospheric O_2 abundance could still have been high perhaps several tens of Myrs after the canonical end of the LJE[28]. In the modern, well-oxygenated world, the geologic O_2 response time is on the order of ~2 Myrs[60], whereas the residence times of Mo, U, and Re in the oceans are ~440, ~400, and ~780 kyrs, respectively[35,40,41]. Therefore, if the LJE decline is linked to a decrease in O_2 production as

196 the result of diminishing C_{org} burial by the end of the LJE, then O_2 would be expected to be
197 significantly attenuated by this time. Instead, our observations provide evidence for the opposite.

198 Our observations provide empirical evidence for models (e.g., ref. 18) that decouple the
199 strongly positive carbonate carbon isotope values of the LJE from enhanced organic carbon
200 burial. Further, if highly oxidized conditions continued up to ~2.0 Ga—or, alternatively, if the
201 Paleoproterozoic experienced large fluctuations in O_2 conditions, the ZF being a zenith—it
202 follows that O_2 abundance was governed by more complex controls than a simple C_{org} burial mass
203 balance, as outlined in Bekker and Holland[4]. This highlights the importance of exploring
204 alternative mechanisms that could account for Paleoproterozoic O_2 accumulation and the need
205 for refined chemostratigraphic and geochronological studies focused on this key interval of
206 Earth's history.

207

208 # Methods

209 ## Materials

210 The material for this study comes from drill cores in the Onega Basin that intersect the ZF—a
211 relatively well-preserved 1500 m-thick succession of organic-rich mudstones and carbonates,
212 interlayered and intersected with igneous units including lavas, tuffs, and sills (see SI for a
213 detailed geological setting)[20,28,63,64]. The 60 m long cores OnZaP-1 and OnZaP-3 were drilled 500
214 m apart in Shunga village, close to drill core FAR-DEEP 13A[27,65]. The 3500 m long OPH core was
215 drilled ~70 km to the south. Paiste *et al.*[27,66] correlated the three cores based on C isotopes, trace
216 metal enrichments, P concentrations, and a distinct massive P-rich dolomite unit that occurs
217 throughout the Onega basin[67].

218 The lithology of this section is characterized by alternating dolomite to calcite-rich
219 carbonates and exceptionally organic-rich mudstones that are intersected by silica or
220 pyrobitumen veins (Figure 1). In the OnZaP section, the interval from the bottom of the core to
221 53 m depth is dominated by highly organic-rich mudstones with relatively few carbonate beds;
222 the 53–33 m interval is mostly dolostone and contains a distinctive dolomite unit; and the 33–1.7

m interval consists of grey mudstones and marly carbonate beds[27]. Two sets of samples from the OnZaP section were analyzed in this study. Set MSP0001 consists of 135 samples that were taken at roughly 1 m intervals and is identical to that used in Paiste *et al.*[27]. Set MSP0010 contains 79 samples that more specifically targeted RSE and organic-rich intervals. A set of 89 samples were analyzed from the 1060–1230 m interval of the OPH core that is roughly equivalent to the OnZaP section.

Elemental concentrations

Total organic carbon content of the MSP0001 and OPH samples were adapted from Paiste *et al.*[27] and were measured from powdered aliquots using a LECO SC-444 analyzer at the Geological Survey of Norway (NGU), Trondheim, Norway. Detection limit was 0.1 wt.% and precision better than 10%. For the MSP0010 set, TOC was measured at the Pôle Spectrométrie Océan, European Institute for Marine Studies (IUEM), Brest, France. Dried and powdered samples were combusted in ceramic beakers at 500 °C for 24h and loss of mass on ignition was determined. Repeat measurements of 7 samples generally differed by <1 wt.%.

Major and trace element compositions of MSP0001 and OPH samples were determined at Acme Labs, Bureau Veritas Commodities Canada Ltd. The samples were first pulverized and combusted to remove organic carbon. For major elements, the sample was fused in $LiBO_2$ flux, then digested, whereas minor elements were analyzed from full digests in HNO_3, $HClO_4$, and HF. Measurements utilized inductively coupled plasma optical emission spectrometry (ICP-OES) or mass spectrometry (ICP-MS). Average relative standard deviation was less than 5% for all elements. MSP0010 element composition was determined at IUEM. Samples were pulverized in a tungsten carbide crusher and an agate mill, then combusted at 500 °C for 24h to remove organic carbon. Major element concentrations were measured on a Jobin Yvon Horiba Ultima 2 ICP-OES after digestion overnight at 80 °C in concentrated HF and HNO_3 and neutralization with boric acid to retain Si. For trace element concentrations, digestion was performed in a class 1000 clean laboratory using distilled acids—samples mixed with concentrated HF and HNO_3 were heated to 80 °C overnight, then allowed to evaporate; this digestion was then repeated with concentrated *aqua regia*, after which the sample was taken up in 6M HCl. Trace element concentrations were

measured on a Thermo Scientific Element 2 ICP-MS calibrated against commercial multi-element standards and digested geostandards (e.g. BHVO-2) were

Samples with a ratio of $(CaO+MgO)/(SiO_2+Al_2O_3) > 0.2$—approximating >20 wt.% carbonate content—were excluded when calculating Mo, U, and Re averages, since compilations of RSE in black shales generally only include shale samples[11,13,26]. An exception was made for samples with >5 wt.% TOC, since such sediments would have played a role in trace metal cycling regardless of their mineralogical composition.

Mo isotopes

Mo isotopes were measured from fully digested OnZaP MSP0010 samples that were purified via column chromatography according to ref. 68. A ^{97}Mo–^{100}Mo double spike was employed[69] and the isotopes were measured on a Thermo Scientific Neptune multi-collector ICP-MS at IFREMER, Brest, France. Data is expressed relative to NIST SRM 3134 = 0.25‰[70]. Detailed methodology is provided in the SI.

U Isotopes

Sample for U isotopes were sequentially digested in a mixture of 3 mL HNO_3 and 1 mL HF at 100ºC for 24 hours, then aqua regia at 95ºC for 24 hours. Following each digestion step the sample was evaporated to dryness. Sample resides were taken up in 5 mL of 3 M HNO_3 at 70ºC. All sample preparation was performed in a Pico-trace clean lab at the Yale Metal Geochemistry Center. Uranium isotope values were measured on a Thermo Neptune Multi-collector ICP-MS following the method in Wang et al., 2018 using the IRMM-3636 URANIUM 233/236 double spike. Accuracy and precision where monitored with concentration matched USGS NOD-A1 and CRM-112A. Error was less than 0.1‰.

Acknowledgements

E. Ponzevera, A. De Prunelé, M.L. Rouget, and K. von Gunten are thanked for help with trace element analyses. KM, KK, AL, TK, PP and KP were supported by the Estonian Science Agency grant PRG447. KM was further supported by the Ministry of Education and Research of Estonia mobility grant within Archimedes Foundation's The Kristjan Jaak Scholarship program "Doctoral Study Abroad"; KP was supported by the Research Council of Norway through its Centres of Excellence funding scheme grant No. 223259; KOK was supported by the Natural Sciences and Engineering Research Council of Canada Discovery grant (RGPIN-165831).

Data availability

The novel ZF geochemical data presented here are included in the supplementary files.

Author contributions

AL, KK, KOK, SVL, and KM conceived the study. KM, KP, TK, AER, KK, and AL conducted field studies and organized the sample acquisition. KP, TK, AER, KK, and AL provided the geological and sedimentary background. KP provided additional TOC data. KM, LJR, SVL, MT, PP, CTR, KL, AV, and KOK measured and interpreted the trace metal abundance data. MT, SVL, and KM analyzed and interpreted the Mo isotope data. NJP, LJR, and KM analyzed and interpreted the U isotope data. SVL, TK, PP and KK analyzed and interpreted *in-situ* trace metal abundance. KM wrote the manuscript with input from all of the co-authors.

Competing interests

The authors declare no competing interests.

References

1. Schidlowski, M., Eichmann, R. & Junge, C. E. Carbon isotope geochemistry of the Precambrian Lomagundi carbonate province, Rhodesia. *Geochim. Cosmochim. Acta* **40**, 449–455 (1976).

2. Martin, A. P., Condon, D. J., Prave, A. R. & Lepland, A. A review of temporal constraints for the Palaeoproterozoic large, positive carbonate carbon isotope excursion (the Lomagundi–Jatuli Event). *Earth-Sci. Rev.* **127**, 242–261 (2013).
3. Karhu, J. A. & Holland, H. D. Carbon isotopes and the rise of atmospheric oxygen. *Geology* **24**, 867–870 (1996).
4. Bekker, A. & Holland, H. D. Oxygen overshoot and recovery during the early Paleoproterozoic. *Earth Planet. Sci. Lett.* **317–318**, 295–304 (2012).
5. Holland, H. D. The oxygenation of the atmosphere and oceans. *Philosophical transactions of the Royal Society of London. Series B, Biological sciences* **361**, 903–15 (2006).
6. Karhu, J. A. *Paleoproterozoic evolution of the carbon isotope ratios of sedimentary carbonates in the Fennoscandian Shield*. (Geologian tutkimuskeskus, 1993).
7. Planavsky, N. J., Bekker, A., Hofmann, A., Owens, J. D. & Lyons, T. W. Sulfur record of rising and falling marine oxygen and sulfate levels during the Lomagundi event. *Proc. Natl. Acad. Sci. U.S.A.* **109**, 18300–5 (2012).
8. Scott, C. *et al.* Pyrite multiple-sulfur isotope evidence for rapid expansion and contraction of the early Paleoproterozoic seawater sulfate reservoir. *Earth Planet. Sci. Lett.* **389**, 95–104 (2014).
9. Blättler, C. L. *et al.* Two-billion-year-old evaporites capture Earth's great oxidation. *Science* eaar2687 (2018). doi:10.1126/science.aar2687
10. Konhauser, K. O. *et al.* Aerobic bacterial pyrite oxidation and acid rock drainage during the Great Oxidation Event. *Nature* **478**, 369–373 (2011).
11. Partin, C. A. *et al.* Large-scale fluctuations in Precambrian atmospheric and oceanic oxygen levels from the record of U in shales. *Earth Planet. Sci. Lett.* **369–370**, 284–293 (2013).
12. Kipp, M. A., Stüeken, E. E., Bekker, A. & Buick, R. Selenium isotopes record extensive marine suboxia during the Great Oxidation Event. *Proc. Natl. Acad. Sci. U.S.A.* 201615867 (2017). doi:10.1073/pnas.1615867114

13. Sheen, A. I. *et al.* A model for the oceanic mass balance of rhenium and implications for the extent of Proterozoic ocean anoxia. *Geochim. Cosmochim. Acta* **227**, 75–95 (2018).
14. Asael, D., Rouxel, O., Poulton, S. W., Lyons, T. W. & Bekker, A. Molybdenum record from black shales indicates oscillating atmospheric oxygen levels in the early Paleoproterozoic. *Am. J. Sci.* **318**, 275–299 (2018).
15. Canfield, D. E. *et al.* Oxygen dynamics in the aftermath of the Great Oxidation of Earth's atmosphere. *Proc. Natl. Acad. Sci. U.S.A.* **110**, 16736–16741 (2013).
16. Bachan, A. & Kump, L. R. The rise of oxygen and siderite oxidation during the Lomagundi Event. *Proc. Natl. Acad. Sci. U.S.A.* **112**, 6562–6567 (2015).
17. Shields, G. A. & Mills, B. J. W. Tectonic controls on the long-term carbon isotope mass balance. *Proc. Natl. Acad. Sci. U.S.A.* 201614506 (2017). doi:10.1073/pnas.1614506114
18. Miyazaki, Y., Planavsky, N., Bolton, E. W. & Reinhard, C. T. Making sense of massive carbon isotope excursions with an inverse carbon cycle model. *J. Geophys. Res. Biogeosci.* **123**, 2485–2496 (2018).
19. Kump, L. R. *et al.* Isotopic evidence for massive oxidation of organic matter following the Great Oxidation Event. *Science* **334**, 1694–1696 (2011).
20. Melezhik, V. A., Fallick, A. E., Filippov, M. M. & Larsen, O. Karelian shungite—an indication of 2.0-Ga-old metamorphosed oil-shale and generation of petroleum: geology, lithology and geochemistry. *Earth-Sci. Rev.* **47**, 1–40 (1999).
21. Strauss, H. *et al.* Enhanced accumulation of organic matter: The Shunga Event. in *Reading the Archive of Earth's Oxygenation* (eds. Melezhik, V. A. et al.) **Volume 3: Global Events and the Fennoscandian Arctic Russia-Drilling Earth Project**, 1195–1273 (Springer, 2013).
22. Zbinden, E. A., Holland, H. D., Feakes, C. R. & Dobos, S. K. The sturgeon falls paleosol and the composition of the atmosphere 1.1 Ga BP. *Precambrian Research* **42**, 141–163 (1988).
23. Planavsky, N. J. *et al.* Low Mid-Proterozoic atmospheric oxygen levels and the delayed rise of animals. *Science* **346**, 635–638 (2014).

24. Tang, D., Shi, X., Wang, X. & Jiang, G. Extremely low oxygen concentration in mid-Proterozoic shallow seawaters. *Precambrian Research* **276**, 145–157 (2016).
25. Bellefroid, E. J. *et al.* Constraints on Paleoproterozoic atmospheric oxygen levels. *PNAS* **115**, 8104–8109 (2018).
26. Reinhard, C. T. *et al.* Proterozoic ocean redox and biogeochemical stasis. *Proc. Natl. Acad. Sci. U.S.A.* **110**, 5357–5362 (2013).
27. Paiste, K. *et al.* Multiple sulphur isotope records tracking basinal and global processes in the 1.98 Ga Zaonega Formation, NW Russia. *Chem. Geol.* **499**, 151–164 (2018).
28. Martin, A. P. *et al.* Multiple Palaeoproterozoic carbon burial episodes and excursions. *Earth Planet. Sci. Lett.* **424**, 226–236 (2015).
29. Melezhik, V. A., Fallick, A. E., Brasier, A. T. & Lepland, A. Carbonate deposition in the Palaeoproterozoic Onega basin from Fennoscandia: a spotlight on the transition from the Lomagundi-Jatuli to Shunga events. *Earth-Sci. Rev.* **147**, 65–98 (2015).
30. Kreitsmann, T. *et al.* Hydrothermal dedolomitisation of carbonate rocks of the Paleoproterozoic Zaonega Formation, NW Russia — Implications for the preservation of primary C isotope signals. *Chemical Geology* **512**, 43–57 (2019).
31. Johnson Ibach, L. E. Relationship Between Sedimentation Rate and Total Organic Carbon Content in Ancient Marine Sediments. *AAPG Bulletin* **66**, 170–188 (1982).
32. Puchtel, I. S. *et al.* Petrology of mafic lavas within the Onega plateau, central Karelia: evidence for 2.0 Ga plume-related continental crustal growth in the Baltic Shield. *Contrib. Mineral. Petrol.* **130**, 134–153 (1998).
33. Puchtel, I. S., Brügmann, G. E. & Hofmann, A. W. Precise Re–Os mineral isochron and Pb–Nd–Os isotope systematics of a mafic–ultramafic sill in the 2.0 Ga Onega plateau (Baltic Shield). *Earth and Planetary Science Letters* **170**, 447–461 (1999).
34. Dunk, R. M., Mills, R. A. & Jenkins, W. J. A reevaluation of the oceanic uranium budget for the Holocene. *Chem. Geol.* **190**, 45–67 (2002).

35. Miller, C. A., Peucker-Ehrenbrink, B., Walker, B. D. & Marcantonio, F. Re-assessing the surface cycling of molybdenum and rhenium. *Geochim. Cosmochim. Acta* **75**, 7146–7179 (2011).
36. Crusius, J., Calvert, S., Pedersen, T. & Sage, D. Rhenium and molybdenum enrichments in sediments as indicators of oxic, suboxic and sulfidic conditions of deposition. *Earth Planet. Sci. Lett.* **145**, 65–78 (1996).
37. Anderson, R. F., Fleisher, M. Q. & LeHuray, A. P. Concentration, oxidation state, and particulate flux of uranium in the Black Sea. *Geochim. Cosmochim. Acta* **53**, 2215–2224 (1989).
38. Algeo, T. J. & Lyons, T. W. Mo–total organic carbon covariation in modern anoxic marine environments: Implications for analysis of paleoredox and paleohydrographic conditions. *Paleoceanography* **21**, PA1016 (2006).
39. Helz, G. R. *et al.* Mechanism of molybdenum removal from the sea and its concentration in black shales: EXAFS evidence. *Geochim. Cosmochim. Acta* **60**, 3631–3642 (1996).
40. Morford, J. L. & Emerson, S. The geochemistry of redox sensitive trace metals in sediments. *Geochim. Cosmochim. Acta* **63**, 1735–1750 (1999).
41. Henderson, G. M. & Anderson, R. F. The U-series Toolbox for Paleoceanography. *Reviews in Mineralogy and Geochemistry* **52**, 493–531 (2003).
42. Och, L. M. & Shields-Zhou, G. A. The Neoproterozoic oxygenation event: Environmental perturbations and biogeochemical cycling. *Earth-Sci. Rev.* **110**, 26–57 (2012).
43. Sahoo, S. K. *et al.* Ocean oxygenation in the wake of the Marinoan glaciation. *Nature* **489**, 546–549 (2012).
44. Lepland, A. *et al.* Potential influence of sulphur bacteria on Palaeoproterozoic phosphogenesis. *Nat. Geosci.* **7**, 20–24 (2014).
45. Morford, J. L., Emerson, S. R., Breckel, E. J. & Kim, S. H. Diagenesis of oxyanions (V, U, Re, and Mo) in pore waters and sediments from a continental margin. *Geochimica et Cosmochimica Acta* **69**, 5021–5032 (2005).

46. Breillat, N., Guerrot, C., Marcoux, E. & Négrel, Ph. A new global database of δ98Mo in molybdenites: A literature review and new data. *J. Geochem. Explor.* **161**, 1–15 (2016).
47. Föllmi, K. B. *et al.* Phosphogenesis and organic-carbon preservation in the Miocene Monterey Formation at Naples Beach, California - The Monterey hypothesis revisited. *Bulletin of the Geological Society of America* **117**, 589–619 (2005).
48. Tribovillard, N., Algeo, T. J., Lyons, T. & Riboulleau, A. Trace metals as paleoredox and paleoproductivity proxies: An update. *Chem. Geol.* **232**, 12–32 (2006).
49. Qu, Y., Črne, A. E., Lepland, A. & van Zuilen, M. A. Methanotrophy in a Paleoproterozoic oil field ecosystem, Zaonega Formation, Karelia, Russia. *Geobiology* **10**, 467–78 (2012).
50. Dickson, A. J. A molybdenum-isotope perspective on Phanerozoic deoxygenation events. *Nature Geosci* **10**, 721–726 (2017).
51. Konhauser, K. O. *et al.* Iron formations: A global record of Neoarchaean to Palaeoproterozoic environmental history. *Earth-Sci. Rev.* **172**, 140–177 (2017).
52. Isley, A. E. & Abbott, D. H. Plume-related mafic volcanism and the deposition of banded iron formation. *J. Geophys. Res. Solid Earth* **104**, 15461–15477 (1999).
53. Holland, H. D. *The Chemical Evolution of the Atmosphere and Oceans*. (Princeton University Press, 1984).
54. Canfield, D. E. A new model for Proterozoic ocean chemistry. *Nature* **396**, 450–453 (1998).
55. Brocks, J. J. *et al.* The rise of algae in Cryogenian oceans and the emergence of animals. *Nature* **548**, 578–581 (2017).
56. Isson, T. T. *et al.* Tracking the rise of eukaryotes to ecological dominance with zinc isotopes. *Geobiology* **16**, 341–352 (2018).
57. Parfrey, L. W., Lahr, D. J. G., Knoll, A. H. & Katz, L. A. Estimating the timing of early eukaryotic diversification with multigene molecular clocks. *Proc. Natl. Acad. Sci. U.S.A.* **108**, 13624–13629 (2011).

58. Betts, H. C. *et al.* Integrated genomic and fossil evidence illuminates life's early evolution and eukaryote origin. *Nat. Ecol. Evol.* **2**, 1556 (2018).
59. El Albani, A. *et al.* Large colonial organisms with coordinated growth in oxygenated environments 2.1 Gyr ago. *Nature* **466**, 100–104 (2010).
60. Kasting, J. F. & Canfield, D. E. The Global Oxygen Cycle. in *Fundamentals of Geobiology* 93–104 (John Wiley & Sons, Ltd, 2012).
61. Melezhik, V. A. *et al.* Emergence of the aerobic biosphere during the Archean-Proterozoic transition: Challenges of future research. *GSA Today* **15**, 4–11 (2005).
62. Ossa Ossa, F. *et al.* Two-step deoxygenation at the end of the Paleoproterozoic Lomagundi Event. *Earth Planet. Sci. Lett.* **486**, 70–83 (2018).
63. Melezhik, V. A., Filippov, M. M. & Romashkin, A. E. A giant Palaeoproterozoic deposit of shungite in NW Russia: genesis and practical applications. *Ore Geol. Rev.* **24**, 135–154 (2004).
64. Melezhik, V. A., Medvedev, P. V. & Svetov, S. A. The Onega Basin. in *Reading the Archive of Earth's Oxygenation* (eds. Melezhik, V. A. et al.) **Volume 1: The Palaeoproterozoic of Fennoscandia As Context for the Fennoscandian Arctic Russia-Drilling Early Earth Project**, 387–490 (Springer, 2013).
65. Črne, A. E. *et al.* Zaonega formation: FAR-DEEP hole 13A. in *Reading the Archive of Earth's Oxygenation* (eds. Melezhik, V. A. et al.) **Volume 2: The Core Archive of the Fennoscandian Arctic Russia-Drilling Early Earth Project**, 1008–1046 (Springer, 2013).
66. Paiste, K. Reconstructing the Paleoproterozoic sulfur cycle: Insights from the multiple sulfur isotope record of the Zaonega Formation, Karelia, Russia. (UiT The Arctic University of Norway, 2018).
67. Črne, A. E. *et al.* Petrography and geochemistry of carbonate rocks of the Paleoproterozoic Zaonega Formation, Russia: Documentation of 13C-depleted non-primary calcite. *Precambrian Res.* **240**, 79–93 (2014).

68. Asael, D. *et al.* Coupled molybdenum, iron and uranium stable isotopes as oceanic paleoredox proxies during the Paleoproterozoic Shunga Event. *Chem. Geol.* **362**, 193–210 (2013).
69. Siebert, C., Nägler, T. F. & Kramers, J. D. Determination of molybdenum isotope fractionation by double-spike multicollector inductively coupled plasma mass spectrometry. *Geochemistry, Geophysics, Geosystems* **2**, (2001).
70. Nägler, T. F. *et al.* Proposal for an international molybdenum isotope measurement standard and data representation. *Geostand Geoanal Res* **38**, 149–151 (2014).
71. Kendall, B., Dahl, T. W. & Anbar, A. D. The stable isotope geochemistry of molybdenum. *Rev. Mineral. Geochem.* **82**, 683–732 (2017).
72. McLennan, S. M. Relationships between the trace element composition of sedimentary rocks and upper continental crust: Trace element composition and upper continental crust. *Geochem. Geophys. Geosyst.* **2**, 1021 (2001).
73. Tissot, F. L. H. & Dauphas, N. Uranium isotopic compositions of the crust and ocean: Age corrections, U budget and global extent of modern anoxia. *Geochimica et Cosmochimica Acta* **167**, 113–143 (2015).
74. Karhu, J. A. Carbon isotopes. in *Geochemistry* 67–73 (Springer, 1999). doi:10.1007/1-4020-4496-8_45
75. Robbins, L. J. *et al.* Trace elements at the intersection of marine biological and geochemical evolution. *Earth-Sci. Rev.* **163**, 323–348 (2016).
76. Wang, X. *et al.* A Mesoarchean shift in uranium isotope systematics. *Geochimica et Cosmochimica Acta* **238**, 438–452 (2018).

297

298

Figure captions

Figure 1: Lithology and geochemistry of the Zaonega Formation. Total organic carbon (TOC) and redox sensitive metal (RSE) profiles, and Mo and U isotope ratios ($\delta^{98/95}$Mo and δ^{238}U) for the OnZaP and OPH sections. Vertical dashed lines are average crustal values[71–73] and the dotted horizontal line is the phosphorous-rich mudstone–dolostone contact used for intra-basinal correlation (see Methods and SI). Boxplots below the Mo and U isotope plots represent the distribution of previously published ZF data from lower in the succession[14,68]. Gray horizontal bands are partly silicified and calcified intervals due to fluid alteration[27]. While these imply the presence of secondary fluids that could have mobilized RSE, microscale RSE distribution confirms the primary nature of the RSE enrichments (see SI).

Figure 2: Secular trends in redox sensitive element concentrations from anoxic shales: Zaonega Formation data plotted on compilations from literature. (a) Changes in $\delta^{13}C_{carb}$ ratio through time, modified from Karhu[74]. (b) Molybdenum concentrations from Robbins *et al.*[75]. (c) Uranium concentrations from Partin *et al.*[11]. (d) Uranium isotope ratios from Wang *et al.*[76], Yang et al. 2017. (e) Rhenium concentrations from Sheen *et al.*[13].

316 Figure 1:

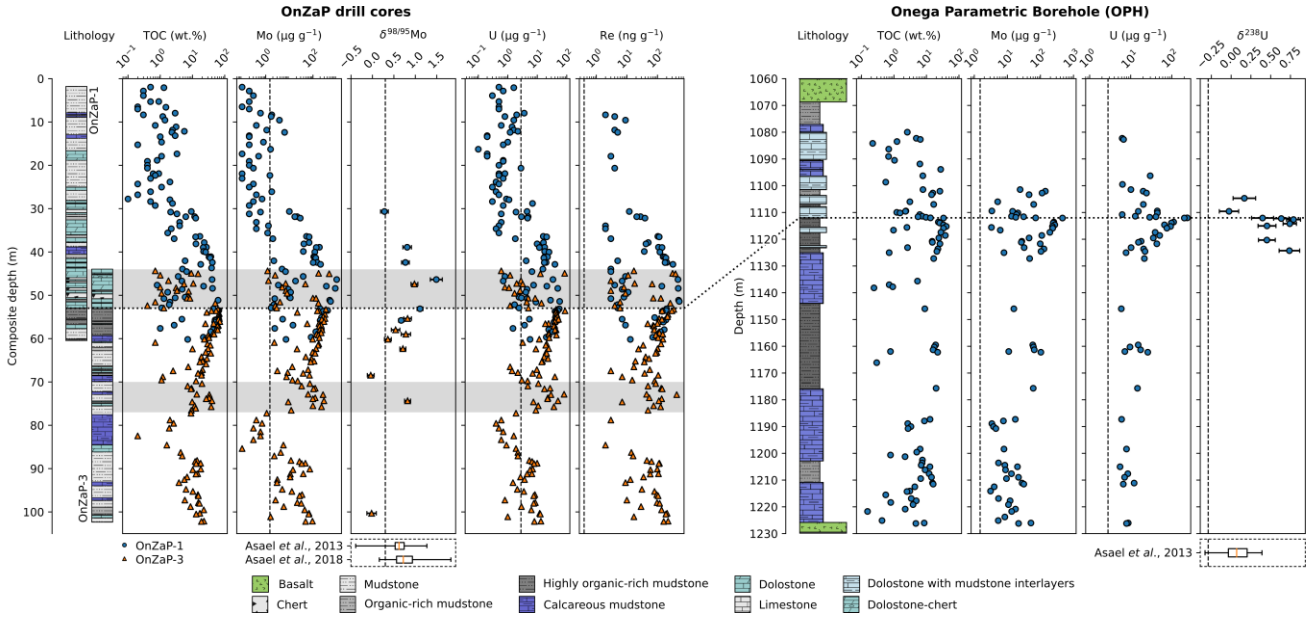

317

318 Figure 2:

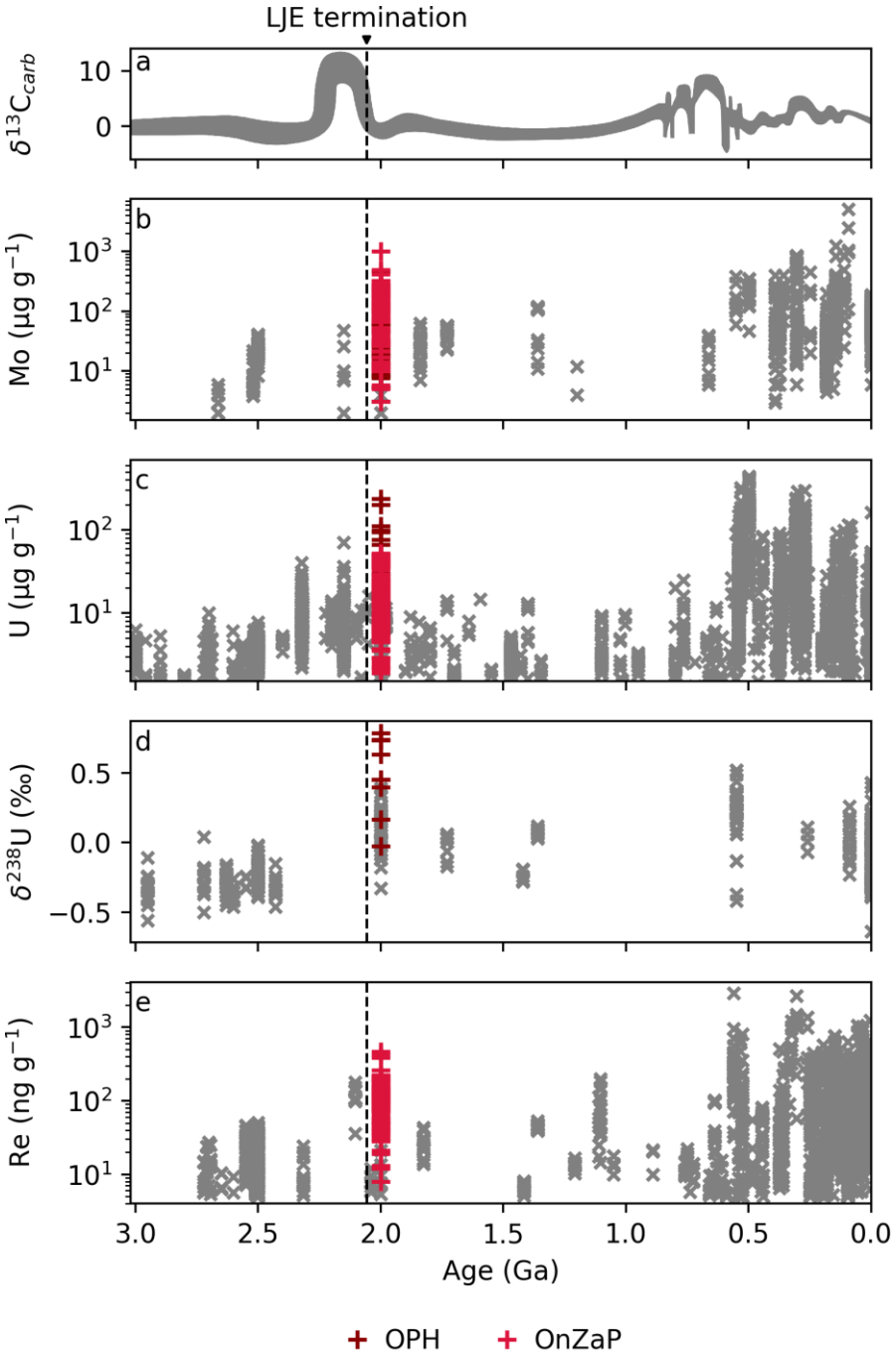
LJE termination
a
b
c
d
e
$\delta^{13}C_{carb}$
Mo (µg g^{-1})
U (µg g^{-1})
δ^{238}U (‰)
Re (ng g^{-1})
10
0
10^3
10^2
10^1
0.5
0.0
−0.5
3.0
2.5
2.0
1.5
1.0
0.5
0.0
Age (Ga)
OPH
OnZaP